Biology of Reproduction, 2018, 99(4), 789–797
doi:10.1093/biolre/ioy105
Research Article
Advance Access Publication Date: 3 May 2018

Research Article

The flagellar protein Enkurin is required for mouse sperm motility and for transport through the female reproductive tract†

Melissa K. Jungnickel[1], Keith A. Sutton[1], Mark A. Baker[2], Michael G. Cohen[1], Michael J. Sanderson[3,‡] and Harvey M. Florman[1,*]

[1]Department of Cell and Developmental Biology, University of Massachusetts Medical School, Worcester, Massachusetts, USA; [2]School of Environmental and Life Sciences, University of Newcastle, Callaghan, New South Wales, Australia and [3]Department of Microbiology and Physiological Systems, University of Massachusetts Medical School, Worcester, Massachusetts, USA

*__Correspondence:__ Department of Cell and Developmental Biology, University of Massachusetts Medical School, 55 Lake Avenue North, Worcester, MA 01655, USA. Tel: +508-856-1675; E-mail: harvey.florman@umassmed.edu

†__Grant Support:__ This work was supported by grants from the NIH (R01 HD046948 to HMF; R03 HD054418 to MKJ) and the NHMRC (APP1101615 to MAB).

‡Deceased Edited by Dr. Jeremy P. Wang, MD, PhD, University of Pennsylvania.

Received 8 October 2017; Revised 18 April 2018; Accepted 1 May 2018

Abstract

Enkurin was identified initially in mouse sperm where it was suggested to act as an intracellular adaptor protein linking membrane calcium influx to intracellular signaling pathways. In order to examine the function of this protein, a targeted mutation was introduced into the mouse *Enkurin* gene. Males that were homozygous for this mutated allele were subfertile. This was associated with lower rates of sperm transport in the female reproductive tract, including reduced entry into the oviduct and slower migration to the site of fertilization in the distal oviduct, and with poor progressive motility in vitro. Flagella from wild-type animals exhibited symmetrical bending and progressive motility in culture medium, and demembranated flagella exhibited the "curlicue" response to Ca^{2+} in vitro. In contrast, flagella of mice homozygous for the mutated allele displayed only asymmetric bending, nonprogressive motility, and a loss of Ca^{2+}-responsiveness following demembrantion. We propose that Enkurin is part of a flagellar Ca^{2+}-sensor that regulates bending and that the motility defects following mutation of the locus are the proximate cause of subfertility.

Summary Sentence

The protein Enkurin is essential for control of flagellar bending and for sperm transport through the female reproductive tract.

Key words: sperm, sperm motility and transport, flagellum, fertilization, male fertility.

Introduction

Enkurin (Enkur) is a conserved protein of flagella and cilia. It was first identified in mouse sperm in a yeast interaction screen using testis transcripts [1], and subsequently detected in the sperm of primates (*Macaca mulatta*) [2], ascidians (*Ciona intestinalis*) [3], bivalves (*Mytilus edulis*) [4], gastropods (*Haliotis rufescens*) [5], and insects (*Drosophila melanogaster*) [6]; in flagella of *Chlamydomonas reinhardtii* [7–9]; and in eukaryote cilia, including those in some mammals [10–13]. Additionally, *ENKUR* plays a role in determining left-right axes in vertebrates, with mutations linked to situs invertus in human and mouse [12, 13]. Misregulation of *Enkur* expression or altered gene copy number is linked to several disease states (the effects of varicocele on sperm [14], Sertoli-cell-only syndrome [15], altered brain endothelial cell function during preeclampsia and eclampsia [16], schizophrenia [17], acute myeloid leukemia [18]) and to partial sterility in *Crassostrea gigas*, the Pacific oyster [19]. Finally,

Enkur orthologs participate in the adaptive response of echinoderm larva to ocean acidification [20], to seasonal variations in *Dreissena polymorpha*, the zebra mussel [21], and to sexual reproduction in the protist *Eimeria tenella* [22].

The domain organization of this protein suggested that it may be an intracellular adapter. The N-terminus contains a proline-rich region with predicted SH3 and WW domain ligand motifs, including an SH3 ligand that binds the regulatory subunit of 1-phosphatidylinositol-3-kinase in vitro. An IQ domain that binds Ca^{2+}/calmodulin but not apo-calmodulin in a cell-free system is present in the central region of the protein. The C-terminal fragment associates with TRPC ion channels in yeast interaction screens. It also contains a predicted coiled-coil domain that may additionally bind other proteins. Based on these sequence and functional features, it was proposed that Enkur participates in the assembly of protein modules during Ca^{2+}-dependent signal transduction [1]. However, there is no direct information on the cellular functions of Enkur. In order to determine the physiological role of this protein we produced a mouse bearing a targeted mutation of the *Enkur* locus. Here, we report the reproductive phenotype of this genetic model.

Methods

Animals

All animal studies followed procedures approved by University of Massachusetts Medical School Institutional Animal Care and Use Committee and comply with Society for the Study of Reproduction guidelines for the care and use of experimental animals. C57BL6 mice (Jackson Laboratory; Bar Harbor, ME) were maintained on 12 h light (0700–1900 h)/12 h dark (1900–0700 h) lighting cycle in the University of Massachusetts Medical School vivarium. Age matched mice used in this study were 6 weeks to 4 months old.

Media and chemicals

Reagents were obtained from the following: Roche (Indianapolis, IN), Bovine Serum and cOmplete Protease Inhibitor Cocktail; EMD Milliipore (Billrica, MA), FHM-HEPES buffered medium and KSOMAA medium for in vitro fertilization; and Sigma-Aldrich (St Louis, MO), all other reagents.

Production and use of antibodies

GST-full length mouse Enkur was subcloned into pThioHis (His-Patch ThioFusion expression system; Invitrogen, MA). Rabbit antisera were generated against recombinant protein and affinity purified according to manufacturer's protocols. Commercial antibodies generated against Enkur were obtained from Enkurin polyclonal antibody (Cat. # PA5-58028; ThermoFisher Scientific, Rockford, IL), and Anti-C10orf63 antibody (Cat. # ab186433; Abcam, Cambridge, MA) (Supplementary Table SI).

Sperm were recovered from caudae epididymides into PBS (pH 7.4). When required, heads and tails were separated by mild proteolysis [23] and membrane integrity of isolated heads was confirmed by Coomassie blue staining [24]. Intact sperm or head and tail fragments from >10-week-old males were washed by sedimentation (700× *g*, 10 min, room temperature), pellets extracted with RIPA buffer (30 min; 4°C), and resedimented (16,000× *g*; 15 min; 4°C). Sperm proteins in supernatant and insoluble fractions were resolved by SDS-polyacrylamide gel electrophoresis, transferred to Immobilon-P membranes, and probed with antibodies, as described previously [1].

Construction of an *Enkur* gene disruption vector

The mouse *Enkur* gene consists of five exons on chromosome 2. Genomic bacterial artificial chromosomes were isolated from a 129S6/SvEvTac library using probes specific for mouse *Enkur* exons 1 and 3. The targeting vector, designed to remove a section of exon 2, consisted of a pKS(-) plasmid containing of a 5′ arm spanning exon 2 and 3 kb of intron 1; a neomycin resistance gene; and a 3′ arm containing 4 kb of intron 2 (Supplementary Figure S1A). Splicing of exon 1 to exon 3 rather than to the trap results in a reading frame shift and would not produce functional protein.

Embryonic stem cells derived from 129/SvJ mice were transfected with linearized DNA and targeted cells were isolated by positive and negative selection with G418 and ganciclovir. Homologous recombination was confirmed by Southern blotting using a 5′ external probe that detects an 8 kb PstI fragment in the wild-type allele and a 6.5-kb PstI fragment in the mutant allele (Supplementary Figure S1B). This probe was generated by the primer pair 5′-TGGACTATGATGCTATGCTC-3′ and 5′-GCTGATAGACACAGCATGAC-3′. The mutated allele is referred to as *Enkur*^{tm}.

Targeted disruption of *Enkur*

Embryonic stem cell clones with an *Enkur*^{tm} allele were injected into C57BL/6J blastocysts in the University of Massachusetts Medical School Transgenic Animal Modeling facility to generate chimeric mice and chimeras were mated to C57BL/6J mice for germline transmission. Mice were maintained on a mixed C56BL/6J-129 background.

PCR genotyping was carried out using genomic DNA derived from tail biopsies with the following primers: a primer homologous to a region upstream of the deleted region that hybridizes with both wild-type and mutant alleles (5′-CCTGGAAAAGATCTCCTTTC-3′); a wild-type allele-specific primer (5′-TATACTCACTGTTTAGAGC-3′); and a mutant allele-specific primer (5′-GTGATATAAACTTGAGGCTG-3′). PCR was performed with rTaq (Promega, Madison, WI) according to manufacturer's instructions and confirmed by Northern hybridization, as described [25], using testis total RNA (s10 μg) extracted from sexually mature (>10 weeks old) males and a mouse *Enkur* full coding region cDNA probe.

Fertility studies

Fertility was determined by cohousing sexually mature C56BL/6J mice for 1–3 months and recording vaginal plugs, pregnancies, and litter size. In vitro fertilization was performed using sperm that were collected from caudae epididymides into FHM medium and capacitated during incubation (1.5 h, 37°C, 5% CO2 in air). Ovulation was induced by sequential intraperitoneal injection of pregnant mare serum gonadotrophin (50 units) and, 46–48 h later, of human chorionic gonadotrophin (50 units). Ovulated oocyte/cumulus complexes were recovered from oviducts 12–14 h after the last injection, incubated with sperm (10^4–10^6/ml; 2 h, 37°C, 5% CO_2 in air) in KSOMAA media, transferred to fresh media, and fertilization was assessed by cleavage to 2-cell after an additional 24-h incubation (37°C, 5% CO_2 in air).

Sperm motility assays

Sperm were collected from caudae epididymides of 12–16-week-old mice into Whitten's medium supplemented with $NaHCO_3$

(20 mM) and bovine serum albumin (1%, w/v), and incubated (37°C, air) for up to 1.5 h. This medium supports sperm capacitation in vitro [26].

Three approaches were used to study sperm motility. Flagellar waveform analysis was carried out in custom-built chambers constructed by placing a thin plastic film (Saran Wrap S.C. Johnson and Co., Racine WI) with a hand-cut channel between a 45 × 50 mm and a 22 × 22 mm cover slip. Sperm were loaded into the channel. Images of loosely tethered sperm pivoting about a single point of attachment of head to coverslip were produced by passing illumination through the differential interference optics (UPlanApo 20X, NA 0.7) of an Olympus IX71 inverted microscope to a charge-coupled device (TM-6740 CL; Pulnix America, Sunnyvale, CA). Images were captured at 200 Hz under instruction of Video Savant software (IO Industries, London, ON, Canada), converted to TIFF format, and analyzed with Volocity 3D (PerkinElmer, Waltham MA) and ImageJ (National Institutes of Health, Bethesda MD) [27]. For each beat cycle, we quantified length of the first flagellar bend as the linear distance from the point where the flagellum-head junction to the first inflection point (see Figure 4c) [28]. We also noted the direction of flagella bends in relation to the orientation of the hook of the mouse sperm head.

Second, sperm movement characteristics were evaluated with Computer Assisted Sperm Analysis (CASA) using a ~100 μm deep chamber prepared with a 2X-CEL insert (Hamilton-Thorne Inc., Beverly, MA) mounted on microscope slides and overlaid with a #1 coverslip. Sperm (2–5 × 10^5/ml) were added to a prewarmed chamber (37°C) and motility recorded at 30-min intervals in an IVOS Analyzer (Version 12, Hamilton-Thorne Inc., Beverley MA), with at least 10 fields recorded per sample.

Finally, flagellar responses to Ca^{2+} were assessed following Triton X-100 extraction, as described by Lindeman and colleagues [29, 30]. The initial 20 μm of flagellum from the head-tail junction was determined using Velocity 3D software and flagellar curvature was defined by the length of a straight line from that point to the head-tail junction.

Analysis of sperm transport in the female reproductive tract

Estrus and ovulation were synchronized in C57Bl6/J females as described [31] and single males were housed with single females for 2 h. Mated females were euthanized and oviducts excised. Sperm entry into the oviduct was determined by dissociating oviducts with collagenase (10 mg/ml in PBS) and by counting sperm by light microscopy. Sperm associated with the cumulus/oocyte complex was determined by isolating those complexes from excised oviducts, by dissociating cumulus masses with hyaluronidase (1 mg/ml in PBS), and by counting total sperm and egg.

Electron microscopy

Cauda epididymal sperm were washed by sedimentation (700× *g*, 10 min). Pellets were embedded in 3% agarose, fixed (2.5% gluteraldehyde, 0.1% cacodylate buffer, 1% tannic acid) overnight, washed in 5% sucrose/0.1M cacodylate buffer (pH 7.4), dehydrated by sequential washes with increasing ethanol concentration, and embedded in Poly/Bed 812 epoxy (Polysciences, Fort Washington PA). Thin sections (80 μm) were cut on a Reichert ultramicrotome, stained with uranyl acetate and lead citrate, and examined using Philips CM10 and CM12 transmission electron microscopes in the Core Electron Microscopy Facility at University of Massachusetts Medical School.

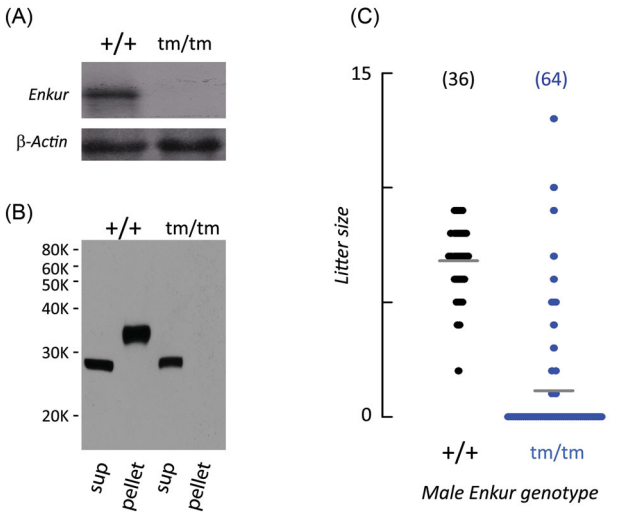

Figure 1. *Enkur*$^{tm/tm}$ mice have decreased male fertility. **(A)** Northern blots reveal an *Enkur* RNA in testis of wild-type mice (+/+) that cannot be detected in mice that are homozygous for the mutated *Enkur* allele (tm/tm). Lower panel: β-actin loading control. **(B)** Immunoblot of sperm proteins. A ~35 kDa band is present in the insoluble fraction (pel) of extracts of wild-type sperm (+/+) but is absent in sperm from mice that are homozygous for the mutant *Enkur* allele (tm/tm). **(C)** Size of litters sired by *Enkur*$^{+/+}$ (+/+) and *Enkur*$^{tm/tm}$ (tm/tm) males during mating with *Enkur*$^{+/+}$ females. Average litter size is indicated (grey horizontal line) and data points represent individual litters. Total number of mating trials is shown above the scatter graph.

Mass spectrometry

Mass spectrometry of sperm proteins was performed as described [32]. Detailed methods are provided in Supplementary Online Information.

Statistical analysis

All values are means ± SD of at least three independent experiments. Statistical analyses were performed using Student's *t*-test (SigmaStat 3.0; Systat Software, San Jose, CA).

Results

Enkur is required for efficient male reproduction

The mouse *Enkur* gene was mutated by replacing part of exon 2 so as to produce a downstream reading frame shift (Supplementary Figure S1). Targeted disruption was confirmed by the absence of transcript in testis of *Enkur*$^{tm/tm}$ mice (Figure 1A). A ~35 kDa protein is present in the insoluble fraction of an extract from *Enkur*$^{+/+}$ sperm and identified as Enkur based on the following: (a) its labeling with an antibody against full length recombinant mouse Enkur (Figure 1B), (b) the presence of an Enkur-specific phospho-peptide, TpMGPAK (residues 48–53, accession NP_082004.1), as demonstrated by mass spectrometry; and (c) in the failure to detect this band in immunoblots of *Enkur*$^{tm/tm}$ sperm (Figure 1B). Enkur migrates more slowly than anticipated based on a deduced molecular weight of 29.6 kDa, possibly due to the known effects of coiled-coil domains, of acidic residues, and of phosphorylation on protein migration in SDS gels [33–36]. A second immunoreactive band of ~28 kDa is

present in the soluble fraction and is retained following disruption of the *Enkur* locus (Figure 1B), but Enkur peptides were not detected in this region of the electrophoretogram. Several commercial antibodies also labeled both the ~35 kDa band that contains Enkur sequences and the apparently nonspecific ~28 kDa band. The presence of this nonspecific immunoreactive band precludes localization of Enkur.

Enkur$^{tm/tm}$ mice were indistinguishable from *Enkur*$^{+/+}$ littermates in body weight (Supplementary Figure S2A), lifespan, appearance, and apparent behavior (data not shown). There was no evident reproductive phenotype of *Enkur* mutation in females, where litter rates and litter sizes were equal to that of wild-type control females. In males there was no effect on testis weight; on the numbers of sperm recovered from caudae epididymides (Supplementary Figure S2B and C); on sperm morphology, including flagellum length (*Enkur*$^{+/+}$, 84.2 ± 1.5 μm; *Enkur*$^{tm/tm}$, 84.3 + 2.3 μm) and gross axonemal morphology (Supplementary Figure S3A and B); or on male mating behavior as assessed by the frequency of copulatory plugs (data not shown). However, as shown in Figure 1C, *Enkur*$^{tm/tm}$ males exhibited severe subfertility; *Enkur*$^{+/+}$ males produced litters in 100% (36/36) of matings, with an average litter size of 6.8 ± 1.6 pups/litter, but the litter rate of *Enkur*$^{tm/tm}$ males was reduced to 20% (13/64 matings) and litter size to 16% (1.1 ± 3.6 pups/litter; $P < 0.01$) of those in wild-type controls. This reduction in average litter size was not due to a small number of males with mutant *Enkur* alleles that had fertility similar to that of wild-type males. Rather, all *Enkur*$^{tm/tm}$ males sired litters at very low frequency.

Enkur is required for efficient sperm transport in the female reproductive tract and fertilization

The persistent ability of *Enkur*$^{tm/tm}$ males to sire litters, even at a low frequency, suggested that sperm from these animals can reach the oviduct ampulla and fertilize oocytes. To test this, we examined the behavior of sperm within the female reproductive tract following mating. Sperm from both *Enkur*$^{+/+}$ and *Enkur*$^{tm/tm}$ males were observed within the oviduct lumen 2 h after mating. However, fewer sperm from *Enkur*$^{tm/tm}$ mice were able to enter the oviduct (n = 4 independent experiments; $P < 0.01$; Figure 2A).

In addition, fertilization in vitro by sperm from *Enkur*$^{tm/tm}$ males was reduced relative to those from wild-type animals by ~85% (10^4 sperm/ml; n = 4 independent experiments; $P < 0.01$; Figure 2B). This relative advantage of wild-type sperm in fertility in vitro was also observed at higher sperm concentrations although genotype-dependent differences were no longer significant, likely reflecting saturation of fertilization as a function of sperm doses [37]. These data show that the fertility defect associated with the loss of *Enkur* function reflects both a failure of sperm transport in the female reproductive tract and also a decreased efficiency of fertilization by those sperm.

Sperm swimming paths are dependent on Enkur function

Sperm from *Enkur*$^{tm/tm}$ mice have a defect in flagellar motility. The first hint came during collection of sperm. Sperm from wild-type animals were extruded from epididymides into culture medium as dense threads that quickly dispersed to produce a uniform suspension, while those from *Enkur*$^{tm/tm}$ males failed to disperse. As the ~35 kDa sperm protein, shown previously to contain an Enkur-specific sequence by mass spectrometry (Figure 1B), is present in tail

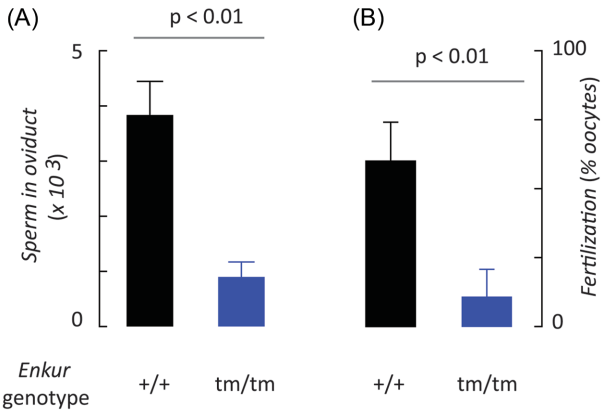

Figure 2. Enkur is critical for sperm transport in the female reproductive tract and fertilization in vitro. Data represents the mean ± SD. **(A)** Numbers of *Enkur*$^{+/+}$ (+/+) and *Enkur*$^{tm/tm}$ (tm/tm) sperm found in the excised oviducts following natural mating (n = 5 independent experiments). **(B)** Fertilization of *Enkur*$^{+/+}$ oocytes (% of total oocytes) in vitro by *Enkur*$^{+/+}$ (+/+) or by *Enkur*$^{tm/tm}$ (tm/tm). Data represents mean ± SD (n = 6 independent experiments). **(A, B)** Horizontal line above bars represents statistical differences by two tailed t-test.

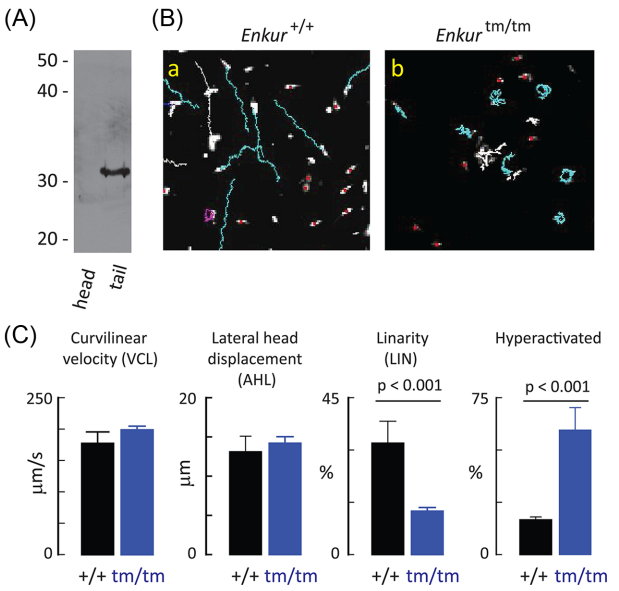

Figure 3. Kinematic effects of Enkur on sperm motility. **(A)** Immunoblot of isolated sperm heads and tails probed with anti-Enkur antibody. Enkur is detected only in the tail fraction. **(B)** Representative CASA traces of *Enkur*$^{+/+}$ and *Enkur*$^{tm/tm}$ sperm following swim out from cauda epididymis. Genotype is indicated above the panels: **Ba**, *Enkur*$^{+/+}$; **Bb**, *Enkur*$^{tm/tm}$. Blue traces represent cases where sperm were tracked continuously during the 20-s acquisition period. This population was used for kinematic analysis. Other colors represent cells that were not tracked continuously throughout the acquisition window and were not analyzed further. **(C)** Kinematic properties of Enkur$^{+/+}$ (five independent experiments, 673 total sperm) and Enkur$^{tm/tm}$ sperm (four independent experiments, 357 total sperm). Fraction of sperm that exhibited hyperactivation-like motility was calculated as described [42]. Data represent means ± SD (horizontal line above bars represents statistical differences by two tailed *t*-test). (Please see the online version for the color figure).

fractions but not in isolated heads (Figure 3A), we next examined the motility of sperm from *Enkur* mutants.

Motility behavior of freely swimming populations was evaluated using a computer-assisted motion tracking system. After release from the cauda epididymis into culture medium $Enkur^{+/+}$ sperm swam along approximately linear paths (Figure 3Ba, blue traces represent tracks of sperm monitored continuously during a 20-s acquisition). In contrast, sperm from animals homozygous for a mutant *Enkur* allele swam in a nonprogressive tumbling or circular pattern (Figure 3Bb). Kinematic analysis of sperm movement revealed no difference in the fraction of sperm exhibiting active motility. Figure 3C shows that sperm from both genotypes has similar velocity of motion along a curvilinear path (VCL) and that lateral head displacement (AHL) was indistinguishable. However, we observed a difference in progressive motility (LIN, an assessment of linearity of cell motion; $Enkur^{+/+}$—673 sperm, five animals; $Enkur^{tm/tm}$—357 sperm, four animals; Figure 3C).

The motility trajectories and kinematic parameters of $Enkur^{tm/tm}$ are suggestive of sperm hyperactivation. In wild-type sperm progressive motility is observed soon after release from the male reproductive tract and is characterized by a low amplitude, symmetric flagellar waveform and a relatively linear swimming path in aqueous media. Hyperactivation is a second mode of flagellar waveform in which higher amplitude and asymmetric bends produce a less progressive type of cell movement. This second flagellar mode is associated with capacitation, a functional reprogramming of sperm that occurs within the female reproductive tract or in an appropriate environment in vitro and that is essential for sperm transport through the female reproductive tract and for fertilization [38–41]. One set of kinematic parameters associated with mouse sperm hyperactivatation include LIN $\leq$ 38, VCL $\geq$ 180, and AHL $\geq$ 9.5 [42]. That set of thresholds, taken alone, suggest that 18 $\pm$ 11% of $Enkur^{+/+}$ sperm had kinematic properties consistent with hyperactivation immediately after release from the male; the population as a whole only develop that second motility pattern with prolonged incubation under capacitating conditions. In contrast, those threshold kinematic parameters suggest that 59 $\pm$ 10% of $Enkur^{tm/tm}$ sperm exhibit swimming properties of hyperactivation swimming at this early time point ($P < 0.001$). In order to explore the potential relationship between *Enkur* function and hyperactivation, we examined flagellar bending patterns directly.

Enkur is critical for normal flagellar motility

Attachment of sperm heads to a glass surface permitted the unencumbered flagellum to be followed through several beat cycles. We additionally determined the wave amplitude and orientation of the primary flagellar bend. Bend orientation is characterized as pro-hook when in the same direction as the concave face of the sperm head and anti-hook bend when away from the concave face [43].

Wild-type sperm produced a flagellar wave in which the primary bend had a low amplitude (12 $\pm$ 6.5 μm from the midline) that alternated between pro-hook and anti-hook orientations. This waveform was initiated at the head-flagellum junction and propagated to the distal flagellar tip (Figure 4Aa1-j1, +/+ uncap rows; Figure 4B, +/+uncap panel; Figure 4C, +/+0 min; Supplementary Movie SM1, right panel). Since curvature of swimming paths increases with flagellar waveform asymmetry [44, 45] these symmetrical waveforms of $Enkur^{+/+}$ sperm immobilized by the head soon after release from the epididymis are consistent with the linear trajectories and kinematic parameters of freely swimming populations

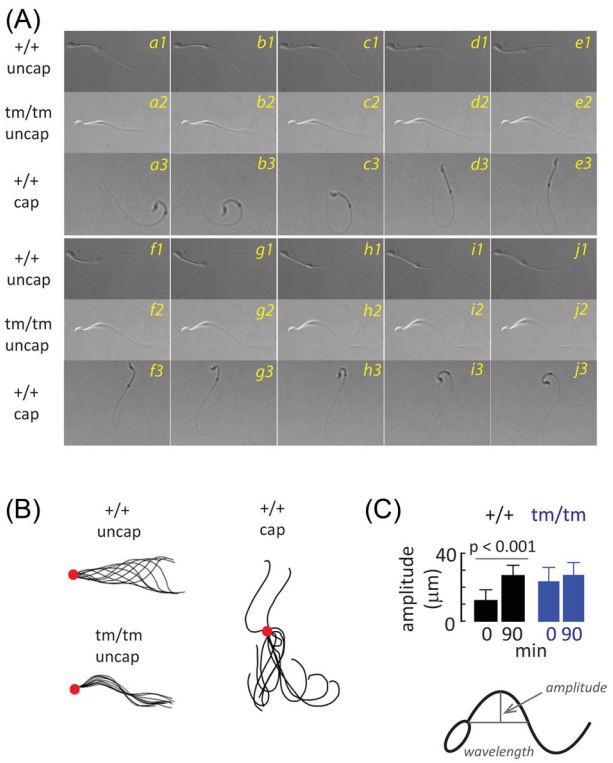

Figure 4. Effects of *Enkur* genotype on flagellar bending. Flagellar motility of uncapacitated cauda epididymal sperm from $Enkur^{+/+}$ (+/+, uncap) and $Enkur^{tm/tm}$ (tm/tm, uncap) mice were examined and compared with $Enkur^{+/+}$ following incubation under capacitating conditions in vitro (+/+, cap). **(A)** A representative montage of flagellar bends (+/+uncap, a1-j1; tm/tm uncap, a2-j2; +/+ cap, a3-j3) with about 33 ms elapsed between frames. **(B)** Traces obtained from montage shown in Panel A. Large circles mark the point where the flagellum contacts the base of the head. (**C**) Primary bend amplitudes of cauda epididymal sperm from $Enkur^{+/+}$ (+/+) and $Enkur^{tm/tm}$ (tm/tm) mice at the beginning of incubation under capacitating conditions and after 90-min incubation. Data represent means $\pm$ SD (horizontal line above bars represents statistical differences by two tailed *t*-test).

(Figure 3B and C). In contrast, $Enkur^{tm/tm}$ sperm displayed a waveform in which the primary bend had a larger amplitude than wild-type sperm (23 + 8.7 μm; Figure 4C, $Enkur^{tm/tm}$ 0 min; $P < 0.001$ compared to $Enkur^{+/+}$) and was markedly asymmetric, consisting exclusively of repetitive pro-hook bends that initiated at the head-flagellum junction (Figure 4Aa2-j2, tm/tm uncap rows; Figure 4B, tm/tm uncap panel; Supplementary Movie SM1, left panel). This asymmetric waveform is consistent with the tumbling, circular swimming paths observed earlier (Figure 3Bb).

Deep, asymmetric flagellar bends in aqueous media are generally a characteristic of sperm hyperactivation [38–40]. Mouse sperm require about 1 h to transition to a capacitated state in vitro and in vivo [46, 47]. We therefore examined the time-dependent development of asymmetric flagellar bending. Figure 4C shows that wild-type sperm display shallow primary bends immediately after release from caudae epididymides and develop a deeper primary bend during a 90-min incubation under capacitating conditions. In contrast, $Enkur^{tm/tm}$ sperm emerge from the epididymis exhibiting the deep primary bend and this does not change during a capacitating incubation.

However, two observations suggest that the altered bending patterns in $Enkur^{tm/tm}$ sperm are not due to a premature hyperactivation. First, a side-by-side comparison shows that flagellar bends

of *Enkur*$^{tm/tm}$ sperm are not similar to those of wild-type sperm that had been capacitated in vitro and that were in a hyperactivated mode. Wild-type sperm have a flexible midpiece and are able to propogate bends to the distal flagellum (Figure 4Aa3-j3, +/+ cap rows; Figure 4B, +/+ cap panel), whereas in mutant sperm the midpiece is markedly stiffer and waves show limited propagation (Figure 4Aa2-j2, tm/tm uncap row; Figure 4B, tm/tm uncap panel). Midpiece stiffness may be a general feature of sperm flagella with a defect in Ca^{2+} signaling as it is seen here with the mutation of Enkur, a Ca^{2+}/calmodulin binding protein [1], as well as in sperm genetic models that lack functional CatSper ion channels due to mutation of *Catsperz* [48], or that lack functional calcineurin following mutation of genes for either catalytic (*Ppp3cc*$^{-/-}$) or regulatory (*Ppp3r2*$^{-/-}$) subunits [49]. Second, hyperactivation is associated with sperm capacitation [50]. To address the possibility that disruption of the *Enkur* locus resulted in accelerated capacitation we examined the time-dependent enhancement of the phosphotyrosine content of a cluster of sperm proteins during incubation under capacitating conditions [51]. The presence of functional Enkur protein had no effect on the development of a phosphoprotein fingerprint during this time period (Supplementary Figure S4). These data suggest that the motility pattern of *Enkur*$^{tm/tm}$ sperm immediately upon release from the epididymis was not due to premature capacitation or a premature hyperaction, but rather a specific effect on flagellar bending.

Role of calcium in *Enkur* phenotype

Disruption of the *Enkur* locus produces sperm with flagellar bending that is markedly asymmetric. Bending asymmetry is regulated by intracellular Ca^{2+} levels [45, 52–55]. The regulatory mechanisms are associated with the flagellum and can be probed following demembranation of sperm with nonionic detergents and reactivation by addition of Mg-ATP [56, 57].

As shown in Figure 5, when mouse sperm plasma membranes are extracted with Triton X-100 and Mg-ATP is added flagella adopt an extended form. The presence of 1 mM Ca^{2+} drives the flagella of >90% of *Enkur*$^{+/+}$ sperm into a highly curved, anti-hook coil (that is, curving opposite the concave face of the sperm head), as described previously by Lindemann and colleagues [30]. In contrast, <15% of *Enkur*$^{tm/tm}$ sperm exhibited a Ca^{2+}-dependent coiled structure (Figure 5).

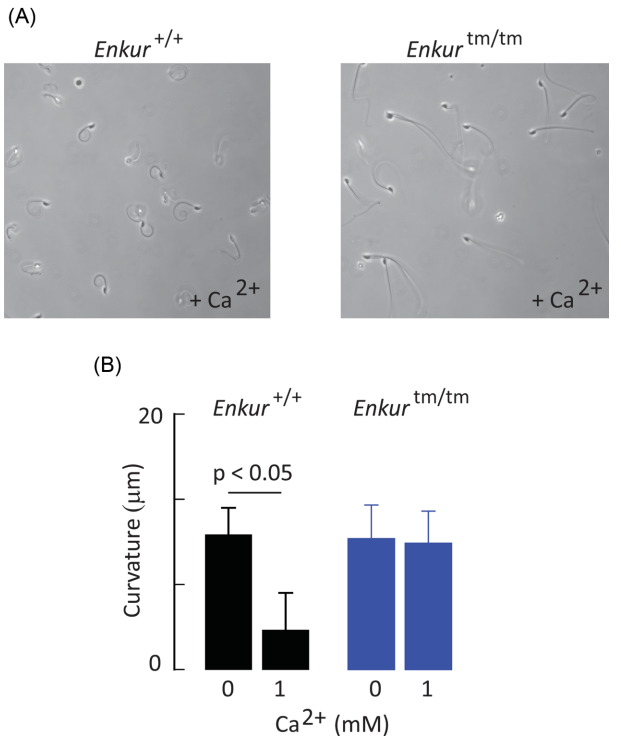

Figure 5. The response of Triton X-100 extracted sperm to Ca^{2+}. (**A**) Representative fields of *Enkur*$^{+/+}$ (left panel) and *Enkur*$^{tm/tm}$ sperm (right panel) following addition of 1 mM $CaCl_2$. Flagella of *Enkur*$^{+/+}$ sperm adopt a highly coiled anti-hook form while those of *Enkur*$^{tm/tm}$ exhibit little or no curvature. **(B)** Curvature is expressed as the straight line distance between the head-flagellum junction and a point on the flagellum 20 μm from the head junction. Flagella of both genotypes were relatively straight in the absence of added Ca^{2+} medium. Following addition of 1 mM Ca^{2+} flagella of *Enkur*$^{+/+}$ sperm become coiled, but there is no observed effect on the flagella of *Enkur*$^{tm/tm}$ sperm. Data represents mean ± SD of five animals for each genotype (>20 sperm were assessed for each animal; horizontal line above bars represents statistical differences by two tailed *t*-test).

Discussion

Here, we report that *Enkur* is required for efficient male fertility. Sperm from animals that are homozygous for a mutated *Enkur* allele show an abnormal motility, emerging from the cauda epididymis with a nonprogressive motility and a highly asymmetric flagellar bending pattern that does not propagate to the distal flagellum efficiently. This pattern is unaltered during prolonged incubation in a capacitating medium. Progressive motility is required for sperm entry into the oviduct [58–60] and so the nonprogressive movement of *Enkur*$^{tm/tm}$ sperm is likely to be the proximate cause of the observed poor transport through the female reproductive tract and of male subfertility.

Sperm from wild-type animals exhibit a very different pattern. Flagella are inert while sperm are stored within caudae epididymides and are first activated in the ejaculate and within proximal regions of the female reproductive tract to produce a relatively symmetrical beat pattern and linear progressive motility. A second flagellar bending pattern, or hyperactivation, appears only after capacitation and is observed only in the oviduct [60]. It is characterized by deep bends and an asymmetric waveform. Development of the hyperactivated mode of bending must be precisely regulated if sperm are to navigate the female reproductive tract, contact eggs and fertilize. Moreover, some forms of mammalian sperm guidance require transitions between symmetric and asymmetric waveforms after capacitation [61, 62].

Transitions between symmetric and asymmetric modes in cilia and in flagella are regulated by intracellular Ca^{2+} (Ca^{2+}_i) activity, as well as by other signaling pathways [55, 63, 64]. In the specific case of mammalian sperm evidence supporting an essential role of flagellar Ca^{2+}_i is based on transient treatment with Ca^{2+} transporting ionophores [65, 66] as well as on the manipulation of cytoplasmic Ca^{2+} clearance pathways [67] and influx channels [68, 69]. At least some of the machinery that control Ca^{2+}-dependent responses is associated directly with the mammalian sperm axoneme and associated structures, as shown by studies with demembranated sperm models [57, 70].

Flagellar Ca^{2+} regulation has been studied extensively in *Chlamydomonas reinhardtii*, *Ciona intestinalis*, and in a number of sea urchins taxa. In those models several Ca^{2+}-binding proteins have been localized to specific regions of the axoneme and proposed as candidate sensors for the control of flagellar function [55, 71–77].

In contrast, relatively little is known about protein mediators of Ca^{2+} response elements of mammalian sperm flagella. Candidates include CABYR, a Ca^{2+} binding protein associated with the fibrous sheath that exhibits increased phosphotyrosine content at the time that hyperactivated motility develops [78]; and calmodulin-dependent protein phosphatase and kinase activities that are associated with the flagellum and linked to Ca^{2+} regulation [79, 80].

We show here that Enkur has some of the anticipated properties of a Ca^{2+} sensor that participates in the regulation of mammalian flagellar bending. Firstly, it is tightly associated with the flagellum. Initial studies, using an antibody directed against a synthetic peptide, indicated that this protein was both in the principal piece of the flagellum and in the acrosomal region of the head in mouse sperm [1]. Here, employing a different antibody (raised against a recombinant, full-length protein), direct proteomic identification and a genetic model that lacks transcript and protein, we confirm the presence of Enkur only in the flagellum. Secondly, disruption of the *Enkur* locus results in a loss of symmetrical bending such that almost all sperm exhibit asymmetrical bending and nonprogressive swimming after release from the cauda epididymis (Figure 4). Bending asymmetry in cilia and flagella is controlled in some way by local Ca^{2+} activities [45, 53, 55] and so the phenotypic effects of Enkur mutation support its proposed role as a Ca^{2+} sensor. Thirdly, Enkur is a Ca^{2+}/calmodulin binding protein [1] and flagella lacking this protein exhibit a loss of Ca^{2+} responsiveness (Figure 5). Calmodulin has been implicated in the Ca^{2+} response of mammalian flagella [81, 82] but the specific targets have not been identified. Taken together, these observations suggest that Enkur can function as a Ca^{2+} sensor in the mouse sperm flagellum. Speculatively, the particular function may involve suppression of asymmetric waves, possibly by dysregulation of dynein switching [83, 84]. Future studies will address such a mechanism as well as the role of this protein in ciliary function.

The behavior of sperm that lack Enkur immediately following recovery from the male is similar in some regard to the flagellar bending and swimming trajectories of capacitated sperm. *Enkur*$^{tm/tm}$ sperm exhibit repetitive pro-hook bends in vitro immediately after release from the cauda epididymis at a time when wild-type sperm show symmetric bends (Figure 4). This bias is identical to that displayed by (wild type) mouse sperm after capacitation in vitro [40, 85]. However, it is now understood that the pro- vs. anti-hook orientation exhibited by sperm following capacitation in the oviduct may differ from that during capacitation in vitro [86]. Moreover, *Enkur*$^{tm/tm}$ sperm lack other indicators of capacitation such as the enhanced protein tyrosine phosphorylation. Finally, a detailed comparison of bending in these mutant sperm with that in wild-type, hyperactivated sperm show that disruption of the *Enkur* locus does not produce premature hyperactivation. We reject the simple hypothesis that mutation of Enkur is sufficient to promote hyperactivation. Instead, it is likely that this protein acts in the sculpting of flagellar bend. Whether this sculpting contributes, with other factors, to the development of hyperactivation is the subject of ongoing investigation.

Our studies demonstrate an essential role of Enkur in the function of mouse sperm flagella. *Enkur*$^{tm/tm}$ mice appear generally to be healthy other than the subfertility of males. The protein is also a component of cilia [10–13], but its role there is not yet understood. It is possible that redundant mechanisms preserve the regulation of ciliary bending following disruption of the *Enkur* locus or, that ciliary functions tolerate loss of asymmetric bending. Alternatively, *Enkur* may provide one more example of a case in which mutations of flagellar/ciliary genes preferentially affect the function of only one of these organelles [87, 88]. Future studies will examine the role of Enkur in cilia directly.

In conclusion, we report that Enkur is required for efficient male fertility in the mouse. More specifically, sperm lacking this protein are compromised in their ability to enter the oviduct, to progress to the site of fertilization, or to fertilize oocytes in vitro. It is essential for the control of flagellar bending patterns in sperm and may play a role in the Ca^{2+}-dependent production of asymmetric bending.

Supplementary data

Supplementary data are available at *BIOLRE* online.

Supplementary Figure S1. Generation of *Enkur*-knockout mice. (**A**) A schematic diagram of the normal *Enkur* allele and the targeted allele. The targeting vector was constructed that replaced part of exon 2 with a neomycin-resistant gene. (**B**) Confirmation of homologous recombination using Southern blotting (*Enkur*$^{+/+}$, +/+; *Enkur*$^{+/tm}$, +/tm; *Enkur*$^{tm/tm}$, tm/tm).

Supplementary Figure S2. General characteristics of *Enkur*$^{+/+}$ and *Enkur*$^{tm/tm}$ male mice. No significant differences were observed between genotypes with regard to (**A**) body weight, (**B**) testis weight, or (**C**) sperm released from the caudae epididymides. Data represent the mean $\pm$ SD (n = 26 *Enkur*$^{+/+}$, 21 *Enkur*$^{-/-}$ males).

Supplementary Figure S3. Flagella parameters of *Enkur*$^{+/+}$ and *Enkur*$^{tm/tm}$ sperm. (**A**) Flagellar lengths did not differ significantly between these genotypes. Data represent the mean $\pm$ SD of observations on flagella from five different males of each genotype (total flagella measured: *Enkur*$^{+/+}$, n = 34; *Enkur*$^{tm/tm}$, n = 41). (**B**) Representative transmission electron micrographs showing cross sections through the sperm principal pieces of *Enkur*$^{+/+}$ and *Enkur*$^{tm/tm}$ mice. No gross morphological differences were apparent.

Supplementary Figure S4. Sperm tyrosine phosphorylation during incubation in vitro under capacitating conditions. Cauda epididymal sperm from *Enkur*$^{+/+}$ (+/+) and *Enkur*$^{tm/tm}$ (tm/tm) were incubated under capacitating conditions for up to 120 min and extracts were probed with an anti-phosphotyrosine antibody. No differences were observed between genotypes were observed. The figure is representative of four independent experiments.

Supplementary Movie SM1. Propagation of flagellar bends in sperm from *Enkur*$^{+/+}$ and *Enkur*$^{-/-}$ mice. Sperm heads were immobilized on glass slides in order to capture flagellar bending. Left panel: *Enkur*$^{tm/tm}$ sperm; right panel: *Enkur*$^{+/+}$ sperm. Images were recorded at 200 frames/s and displayed at 30 frames/s. See Figure 4 (main text) for an analysis of bending pattern.

Supplementary Table SI. Antibody resources.

References

1. Sutton KA, Jungnickel MK, Wang Y, Cullen K, Lambert S, Florman HM. Enkurin is a novel calmodulin and TRPC channel binding protein in sperm. *Dev Biol* 2004; **274**(2):426–435.
2. Skerget S, Rosenow M, Polpitiya A, Petritis K, Dorus S, Karr TL. The Rhesus macaque (Macaca mulatta) sperm proteome. *Mol Cell Proteomics* 2013; **12**(11):3052–3067.
3. Nakachi M, Nakajima A, Nomura M, Yonezawa K, Ueno K, Endo T, Inaba K. Proteomic profiling reveals compartment-specific, novel functions of ascidian sperm proteins. *Mol Reprod Dev* 2011; **78**:529–549.
4. Bartel M, Hartmann S, Lehmann K, Postel K, Quesada H, Philipp EER, Heilmann K, Micheel B, Stuckas H. Identification of sperm proteins as candidate biomarkers for the analysis of reproductive isolation in *Mytilus*: a case study for the enkurin locus. *Mar Biol* 2012; **159**(10):2195–2207.

5. Palmer MR, McDowall MH, Stewart L, Ouaddi A, MacCoss MJ, Swanson WJ. Mass spectrometry and next-generation sequencing reveal an abundant and rapidly evolving abalone sperm protein. *Mol Reprod Dev* 2013; **80**:460–465.
6. Wasbrough ER, Dorus S, Hester S, Howard-Murkin J, Lilley K, Wilkin E, Polpitiya A, Petritis K, Karr TL. The Drosophila melanogaster sperm proteome-II (DmSP-II). *J Proteomics* 2010; **73**(11):2171–2185.
7. Li JB, Gerdes JM, Haycraft CJ, Fan Y, Teslovich TM, May-Simera H, Li H, Blacque OE, Li L, Leitch CC, Lewis RA, Green JS, et al. Comparative genomics identifies a flagellar and basal body proteome that includes the BBS5 human disease gene. *Cell* 2004; **117**(4):541–552.
8. Pazour GJ, Agrin N, Leszyk J, Witman GB. Proteomic analysis of a eukaryotic cilium. *J Cell Biol* 2005; **170**(1):103–113.
9. Stolc V, Samanta MP, Tongprasit W, Marshall WF. Genome-wide transcriptional analysis of flagellar regeneration in *Chlamydomonas reinhardtii* identifies orthologs of ciliary disease genes. *Proc Natl Acad Sci* 2005; **102**(10):3703–3707.
10. Ross AJ, Dailey LA, Brighton LE, Devlin RB. Transcriptional profiling of mucociliary differentiation in human airway epithelial cells. *Am J Respir Cell Mol Biol* 2007; **37**(2):169–185.
11. Lai CK, Gupta N, Wen X, Rangell L, Chih B, Peterson AS, Bazan JF, Li L, Scales SJ. Functional characterization of putative cilia genes by high-content analysis. *Mol Biol Cell* 2011; **22**(7):1104–1119.
12. Stauber M, Weidemann M, Dittrich-Breiholz O, Lobschat K, Alten L, Mai M, Beckers A, Kracht M, Gossler A. Identification of FOXJ1 effectors during ciliogenesis in the foetal respiratory epithelium and embryonic left-right organiser of the mouse. *Dev Biol* 2017; **423**(2):170–188.
13. Sigg MA, Menchen T, Lee C, Johnson J, Jungnickel MK, Choksi SP, Garcia GR, Busengdal H, Dougherty GW, Pennekamp P, Werner C, Rentzsch F, et al. Evolutionary proteomics uncovers ancient associations of cilia with signaling pathways. *Dev Cell* 2017; **43**(6):744–762.e11.
14. Agarwal A, Sharma R, Durairajanayagam D, Cui Z, Ayaz A, Gupta S, Willard B, Gopalan B, Sabanegh E. Spermatozoa protein alterations in infertile men with bilateral varicocele. *Asian J Androl* 2016; **18**(1):43–53.
15. Tuttelmann F, Simoni M, Kliesch S, Ledig S, Dworniczak B, Wieacker P, Ropke A. Copy number variants in patients with severe oligozoospermia and Sertoli-cell-only syndrome. *PLoS One* 2011; **6**(4):e19426.
16. Ing NH, Berghman L, Abi-Ghanem D, Abbas K, Kaush A, Riggs PK, Puschett JB. Marinobufagenin regulates permeability and gene expression of brain endothelial cells. *Am J Physiol Regul Integr Comp Physiol* 2014; **306**(12):R918–R924.
17. Carroll AP, Tooney PA, Cairns MJ. Design and interpretation of microRNA–reporter gene activity. *Anal Biochem* 2013; **437**(2):164–171.
18. Hatfield K, Oyan AM, Ersvaer E, Kalland KH, Lassalle P, Gjertsen BT, Bruserud O. Primary human acute myeloid leukaemia cells increase the proliferation of microvascular endothelial cells through the release of soluble mediators. *Br J Haematol* 2009; **144**(1):53–68.
19. Dheilly NM, Jouaux A, Boudry P, Favrel P, Lelong C. Transcriptomic profiling of gametogenesis in triploid Pacific Oysters Crassostrea gigas: towards an understanding of partial sterility associated with triploidy. *PLoS One* 2014; **9**(11):e112094.
20. Evans TG, Chan F, Menge BA, Hofmann GE. Transcriptomic responses to ocean acidification in larval sea urchins from a naturally variable pH environment. *Mol Ecol* 2013; **22**(6):1609–1625.
21. Navarro A, Campos B, Barata C, Pina B. Transcriptomic seasonal variations in a natural population of zebra mussel (Dreissena polymorpha). *Sci Total Environ* 2013; **454–455**:482–489.
22. Walker RA, Sharman PA, Miller CM, Lippuner C, Okoniewski M, Eichenberger RM, Ramakrishnan C, Brossier F, Deplazes P, Hehl AB, Smith NC. RNA Seq analysis of the Eimeria tenella gametocyte transcriptome reveals clues about the molecular basis for sexual reproduction and oocyst biogenesis. *BMC Genomics* 2015; **16**(1):94.
23. Millette CF, Spear PG, Gall WE, Edelman GM. Chemical dissection of mammalian spermatozoa. *J Cell Biol* 1973; **58**(3):662–675.
24. Moller CC, Bleil JD, Kinloch RA, Wassarman PM. Structural and functional relationships between mouse and hamster zona pellucida glycoproteins. *Dev Biol* 1990; **137**(2):276–286.
25. Sutton KA, Vu MN, Wilkinson MF. Distal V beta promoters transcribe novel T-cell receptor-beta transcripts in early development. *Immunology* 1998; **93**(2):213–220.
26. Jungnickel MK, Sutton KA, Wang Y, Florman HM. Phosphoinositide-dependent pathways in mouse sperm are regulated by egg ZP3 and drive the acrosome reaction. *Dev Biol* 2007; **304**(1):116–126.
27. Schneider CA, Rasband WS, Eliceiri KW. NIH Image to ImageJ: 25 years of image analysis. *Nat Methods* 2012; **9**:671–675.
28. Ho HC, Granish KA, Suarez SS. Hyperactivated motility of bull sperm is triggered at the axoneme by Ca^{2+} and not cAMP. *Dev Biol* 2002; **250**(1):208–217.
29. Lindemann CB, Lesich KA. Detergent-extracted models for the study of cilia or flagella. *Methods Mol Biol* 2009; **586**:337–353.
30. Lesich KA, Kelsch CB, Ponichter KL, Dionne BJ, Dang L, Lindemann CB. The calcium response of mouse sperm flagella: role of calcium ions in the regulation of dynein activity. *Biol Reprod* 2012; **86**(4):105.
31. Sutton KA, Jungnickel MK, Florman HM. A polycystin-1 controls post-copulatory reproductive selection in mice. *Proc Natl Acad Sci* 2008; **105**(25):8661–8666.
32. Baker MA, Witherdin R, Hetherington L, Cunningham-Smith K, Aitken RJ. Identification of post-translational modifications that occur during sperm maturation using difference in two-dimensional gel electrophoresis. *Proteomics* 2005; **5**(4):1003–1012.
33. Matagne A, Joris B, Frere JM. Anomalous behaviour of a protein during SDS/PAGE corrected by chemical modification of carboxylic groups. *Biochem J* 1991; **280**(2):553–556.
34. Graceffa P, Jancso A, Mabuchi K. Modification of acidic residues normalizes sodium dodecyl sulfate-polyacrylamide gel electrophoresis of caldesmon and other proteins that migrate anomalously. *Arch Biochem Biophys* 1992; **297**(1):46–51.
35. Koutoulis A, Pazour GJ, Wilkerson CG, Inaba K, Sheng H, Takada S, Witman GB. The *Chlamydomonas reinhardtii* ODA3 gene encodes a protein of the outer dynein arm docking complex. *J Cell Biol* 1997; **137**(5):1069–1080.
36. Wirschell M, Pazour G, Yoda A, Hirono M, Kamiya R, Witman GB. Oda5p, a novel axonemal protein required for assembly of the outer dynein arm and an associated adenylate kinase. *Mol Biol Cell* 2004; **15**(6):2729–2741.
37. Wolf DP, Inoue M. Sperm concentration dependency in the fertilization and zonae sperm binding properties of mouse eggs inseminated in vitro. *J Exp Zool* 1976; **196**(1):27–37.
38. Yanagimachi R. The movement of golden hamster spermatozoa before and after capacitation. *Reproduction* 1970; **23**(1):193–196.
39. Katz DF, Drobnis EZ, Overstreet JW. Factors regulating mammalian sperm migration through the female reproductive tract and oocyte vestments. *Gamete Res* 1989; **22**(4):443–469.
40. Chang H, Suarez SS. Rethinking the relationship between hyperactivation and chemotaxis in mammalian sperm. *Biol Reprod* 2010; **83**(4):507–513.
41. Florman HM, Fissore R. Fertilization in mammals. In: Plant TM, Zeleznik AJ (eds.), *Knobil and Neill's Physiology of Reproduction*, 4th ed. San Diego: Elsevier; 2015: 149–196.
42. Bray C, Son JH, Kumar P, Meizel S. Mice deficient in CHRNA7, a subunit of the nicotinic acetylcholine receptor, produce sperm with impaired motility. *Biol Reprod* 2005; **73**(4):807–814.
43. Ishijima S, Baba SA, Mohri H, Suarez SS. Quantitative analysis of flagellar movement in hyperactivated and acrosome-reacted golden hamster spermatozoa. *Mol Reprod Dev* 2002; **61**(3):376–384.
44. Goldstein SF. Asymmetric waveforms in echinoderm sperm flagella. *J Exp Biol* 1977; **71**:157–170.
45. Brokaw CJ. Calcium-induced asymmetrical beating of triton-demembranated sea urchin sperm flagella. *J Cell Biol* 1979; **82**(2):401–411.
46. Iwamatsu T, Chang MC. Further investigation of capacitation of sperm and fertilization of mouse eggsin vitro. *J Exp Zool* 1970; **175**(3):271–281.
47. Austin CR. Principles of fertilization. *Proc R Soc Med* 1974; **67**:925–927.
48. Chung JJ, Miki K, Kim D, Shim SH, Shi HF, Hwang JY, Cai X, Iseri Y, Zhuang X, Clapham DE. CatSperzeta regulates the structural continuity

of sperm Ca(2+) signaling domains and is required for normal fertility. *Elife* 2017; **6**:e23082.
49. Miyata H, Satouh Y, Mashiko D, Muto M, Nozawa K, Shiba K, Fujihara Y, Isotani A, Inaba K, Ikawa M. Sperm calcineurin inhibition prevents mouse fertility with implications for male contraceptive. *Science* 2015; **350**(6259):442–445.
50. Yanagimachi R. Mammalian fertilization. In: Knobil E, Neill JD (eds.), *The Physiology of Reproduction*, 2nd ed. New York: Raven Press, Ltd.; 1994: 189–317.
51. Visconti PE, Bailey JL, Moore GD, Pan D, Olds-Clarke P, Kopf GS. Capacitation of mouse spermatozoa. I. Correlation between the capacitation state and protein tyrosine phosphorylation. *Development* 1995; **121**:1129–1137.
52. Brokaw CJ, Josslin R, Bobrow L. Calcium ion regulation of flagellar beat symmetry in reactivated sea urchin spermatozoa. *Biochem Biophys Res Commun* 1974; **58**(3):795–800.
53. Lindemann CB, Goltz JS. Calcium regulation of flagellar curvature and swimming pattern in triton X-100-extracted rat sperm. *Cell Motil Cytoskeleton* 1988; **10**(3):420–431.
54. Alvarez L, Friedrich BM, Gompper G, Kaupp UB. The computational sperm cell. *Trends Cell Biol* 2014; **24**(3):198–207.
55. Inaba K. Calcium sensors of ciliary outer arm dynein: functions and phylogenetic considerations for eukaryotic evolution. *Cilia* 2015; **4**(1):6.
56. Gibbons BH, Gibbons IR. Flagellar movement and adenosine triphosphatase activity in sea urchin sperm extracted with triton X-100. *J Cell Biol* 1972; **54**(1):75–97.
57. Lindemann CB, Gibbons IR. Adenosine triphosphate-induced motility and sliding of filaments in mammalian sperm extracted with Triton X-100. *J Cell Biol* 1975; **65**(1):147–162.
58. Gaddum-Rosse P. Some observations on sperm transport through the uterotubal junction of the rat. *Am J Anat* 1981; **160**(3):333–341.
59. Shalgi R, Smith TT, Yanagimachi R. A quantitative comparison of the passage of capacitated and uncapacitated hamster spermatozoa through the uterotubal junction. *Biol Reprod* 1992; **46**(3):419–424.
60. Suarez SS. Gamete and zygote transport. In: Plant TM, Zeleznik AJ (eds.), *Knobil and Neill's Physiology and Reproduction*, 4th ed. San Diego: Elsevier; 2015: 197–232.
61. Perez-Cerezales S, Boryshpolets S, Eisenbach M. Behavioral mechanisms of mammalian sperm guidance. *Asian J Androl* 2015; **17**:628–632.
62. Boryshpolets S, Perez-Cerezales S, Eisenbach M. Behavioral mechanism of human sperm in thermotaxis: a role for hyperactivation. *Hum Reprod* 2015; **30**(4):884–892.
63. Witman GB. *Chlamydomonas* phototaxis. *Trends Cell Biol* 1993; **3**(11):403–408.
64. Woolley DM. Flagellar oscillation: a commentary on proposed mechanisms. *Biol Rev Camb Philos Soc* 2010; **85**:453–470.
65. Suarez SS, Vincenti L, Ceglia MW. Hyperactivated motility induced in mouse sperm by calcium ionophore A23187 is reversible. *J Exp Zool* 1987; **244**(2):331–336.
66. Tateno H, Krapf D, Hino T, Sanchez-Cardenas C, Darszon A, Yanagimachi R, Visconti PE. Ca2+ ionophore A23187 can make mouse spermatozoa capable of fertilizing in vitro without activation of cAMP-dependent phosphorylation pathways. *Proc Natl Acad Sci* 2013; **110**(46):18543–18548.
67. Okunade GW, Miller ML, Pyne GJ, Sutliff RL, O'Connor KT, Neumann JC, Andringa A, Miller DA, Prasad V, Doetschman T, Paul RJ, Shull GE. Targeted ablation of plasma membrane Ca2+-ATPase isoforms 1 and 4 indicates a critical role in hyperactivated sperm motility and male fertility for PMCA4. *J Biol Chem* 2004; **279**(32):33742–33750.
68. Carlson AE, Westenbroek RE, Quill T, Ren D, Clapham DE, Hille B, Garbers DL, Babcock DF. CatSper1 required for evoked Ca2+ entry and control of flagellar function in sperm. *Proc Natl Acad Sci* 2003; **100**(25):14864–14868.
69. Lishko PV, Kirichok Y, Ren D, Navarro B, Chung JJ, Clapham DE. The control of male fertility by spermatozoan ion channels. *Annu Rev Physiol* 2012; **74**(1):453–475.
70. Lindemann CB, Lesich KA. Functional anatomy of the mammalian sperm flagellum. *Cytoskeleton* 2016; **73**(11):652–669.
71. King SM, Patel-King RS. Identification of a Ca(2+)-binding light chain within *Chlamydomonas* outer arm dynein. *J Cell Sci* 1995; **108**(Pt 12):3757–3764.
72. Yang P, Diener DR, Rosenbaum JL, Sale WS. Localization of calmodulin and dynein light chain LC8 in flagellar radial spokes. *J Cell Biol* 2001; **153**:1315–1326.
73. Yang P, Diener DR, Yang C, Kohno T, Pazour GJ, Dienes JM, Agrin NS, King SM, Sale WS, Kamiya R, Rosenbaum JL, Witman GB. Radial spoke proteins of *Chlamydomonas flagella*. *J Cell Sci* 2006; **119**:1165–1174.
74. Sakato M, Sakakibara H, King SM. *Chlamydomonas* outer arm dynein alters conformation in response to Ca2+. *Mol Biol Cell* 2007; **18**:3620–3634.
75. Mizuno K, Padma P, Konno A, Satouh Y, Ogawa K, Inaba K. A novel neuronal calcium sensor family protein, calaxin, is a potential Ca2+-dependent regulator for the outer arm dynein of metazoan cilia and flagella. *Biol Cell* 2009; **101**:91–103.
76. King SM. Sensing the mechanical state of the axoneme and integration of Ca2+ signaling by outer arm dynein. *Cytoskeleton (Hoboken)* 2010; **67**:207–213.
77. Brown JM, Dipetrillo CG, Smith EF, Witman GB. A FAP46 mutant provides new insights into the function and assembly of the C1d complex of the ciliary central apparatus. *J Cell Sci* 2012; **125**:3904–3913.
78. Naaby-Hansen S, Mandal A, Wolkowicz MJ, Sen B, Westbrook VA, Shetty J, Coonrod SA, Klotz KL, Kim YH, Bush LA, Flickinger CJ, Herr JC. CABYR, a novel calcium-binding tyrosine phosphorylation-regulated fibrous sheath protein involved in capacitation. *Dev Biol* 2002; **242**:236–254.
79. Tash JS, Krinks M, Patel J, Means RL, Klee CB, Means AR. Identification, characterization, and functional correlation of calmodulin-dependent protein phosphatase in sperm. *J Cell Biol* 1988; **106**:1625–1633.
80. Ignotz GG, Suarez SS. Calcium/calmodulin and calmodulin kinase II stimulate hyperactivation in demembranated bovine sperm. *Biol Reprod* 2005; **73**:519–526.
81. Tash JS, Means AR. Regulation of protein phosphorylation and motility of sperm by cyclic adenosine monophosphate and calcium. *Biol Reprod* 1982; **26**:745–763.
82. Lindemann CB, Gardner TK, Westbrook E, Kanous KS. The calcium-induced curvature reversal of rat sperm is potentiated by cAMP and inhibited by anti-calmodulin. *Cell Motil Cytoskeleton* 1991; **20**:316–324.
83. Mitchison TJ, Mitchison HM. How cilia beat. *Nature* 2010; **463**:308–309.
84. Satir P, Heuser T, Sale WS. A structural basis for how motile cilia beat. *Bioscience* 2014; **64**:1073–1083.
85. Fraser LR. Motility patterns in mouse spermatozoa before and after capacitation. *J Exp Zool* 1977; **202**:439–444.
86. Chang H, Suarez SS. Unexpected flagellar movement patterns and epithelial binding behavior of mouse sperm in the oviduct. *Biol Reprod* 2012; **140**:1–8.
87. Zhang Z, Kostetskii I, Tang W, Haig-Ladewig L, Sapiro R, Wei Z, Patel AM, Bennett J, Gerton GL, Moss SB, Radice GL, Strauss JF, III. Deficiency of SPAG16L causes male infertility associated with impaired sperm motility. *Biol Reprod* 2006; **74**:751–759.
88. Lo JC, Jamsai D, O'Connor AE, Borg C, Clark BJ, Whisstock JC, Field MC, Adams V, Ishikawa T, Aitken RJ, Whittle B, Goodnow CC, et al. RAB-like 2 has an essential role in male fertility, sperm intra-flagellar transport, and tail assembly. *PLoS Genet* 2012; **8**:e1002969.